

## Chapter 2

# Sequential Forward Solver

**Abstract** In this chapter, the theory of the inverse and direct (forward) scattering problem is explained. A method for solving the inverse problem is developed in detail, and the results of some numerical simulations are used to make an in-depth analysis of the capabilities and effectiveness of the proposed approach.

### 2.1 Maxwell's Equations

MWT is the process of creating the image of dielectric properties from measured electric field qualities. The dielectric properties and measured field are related by a nonlinear relationship that is modeled by Maxwell's equations. The time-harmonic Maxwell's equations describe the electromagnetic phenomena in macroscopic media and are given by [1]:

$$\nabla \times \mathbf{E}(\mathbf{r}) = -j\omega\mathbf{B}(\mathbf{r}) \quad \text{Farady's law,} \quad (2.1)$$

$$\nabla \times \mathbf{H}(\mathbf{r}) = j\omega\mathbf{D}(\mathbf{r}) + \mathbf{J}(\mathbf{r}) \quad \text{Ampere's law,} \quad (2.2)$$

$$\nabla \cdot \mathbf{B}(\mathbf{r}) = 0 \quad \text{Gauss' law,} \quad (2.3)$$

$$\nabla \cdot \mathbf{D}(\mathbf{r}) = \rho \quad \text{Gauss' law,} \quad (2.4)$$

where  $\mathbf{E}$  (V/m) is the electric field intensity,  $\mathbf{H}$  (A/m) is the magnetic field intensity,  $\mathbf{B}$  (T) is the magnetic flux density,  $\mathbf{D}$  (C/m<sup>2</sup>) is the electric flux density,  $\mathbf{J}$  (A/m<sup>2</sup>) is the electric current density (in phasor format),  $\rho$  (C/m<sup>3</sup>) is electric charge density,  $\mathbf{r}$  denotes the position vector,  $j = \sqrt{-1}$  is the imaginary unit, and  $\omega = 2\pi f$  (rad/Hz) is the radial frequency ( $f$  is the frequency). In order to include the information about the media in which electromagnetic phenomena occur, the *constitutive relations* have been used. Thus, for an isotropic and linear medium (background and OI), the relationships between the vector field and the medium become

$$\mathbf{D}(\mathbf{r}) = \epsilon_r \epsilon_0 \mathbf{E}(\mathbf{r}), \quad (2.5)$$

$$\mathbf{B}(\mathbf{r}) = \mu_0 \mu_r \mathbf{H}(\mathbf{r}), \quad (2.6)$$

$$\mathbf{J}(\mathbf{r}) = \sigma \mathbf{E}(\mathbf{r}), \quad (2.7)$$

where  $\epsilon_0$  (F/m) is the permittivity of free space,  $\epsilon_r$  (unit-less) is the relative permittivity (dielectric constant),  $\mu_0$  (H/m) is the permeability of free space,  $\mu_r$  (unit-less) is the relative permeability, and  $\sigma$  (S/m) is the electrical conductivity. We consider nonmagnetic media in this book ( $\mu_r = 1.0$ ). The value of permittivity and conductivity may depend on the operating frequency. This dependency can be modeled by different formulas. In this book the Debye model has been used. Substituting Eqs. (2.5)–(2.7) into Eqs. (2.1)–(2.4), what can be seen is the dependency of the electric field on dielectric properties of the background. Solving the Maxwell's equations in order to determine the electric field ( $\mathbf{E}$ ) from the knowledge of the source ( $\mathbf{J}$ ), obstacles, and medium dielectric properties ( $\epsilon_r, \sigma$ ) is called the forward scattering problem. The forward problem may be solved based on either IE formulation [2] or PDE formulation. In contrast, in an inverse scattering problem, the goal is to determine the physical quantities of the media ( $\epsilon_r, \sigma$ ) from the knowledge of the electric field ( $\mathbf{E}$ ) at a set of receiver points and knowledge of the source ( $\mathbf{J}$ ).

In the following sections, some challenges associated with the inverse scattering problem are explained, and some solutions are provided for them. The inverse scattering problem is always associated with ill-posedness and nonlinearity. The next section is devoted to introducing these two characteristics for the inverse problem.

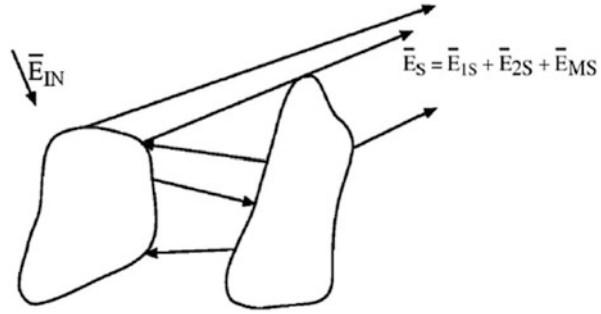
### 2.1.1 Ill-Posedness of the Inverse Problem

In regards to ill-posedness, in the sense of Hadamard [3], any problem is considered a well-posed problem if the solution is:

- I. *In Existence*: For the existence of the solution (i.e., map of dielectric properties of scatterers), as long as the best approximations are made for solving the mathematical model, we can guarantee that a solution exists.
- II. *Unique*: For the uniqueness of the solution, based upon the Maxwell's equations, the scattered fields are continuous functions of incident field and dielectric properties of the background.

Therefore, the solution is unique if the knowledge of the scattering field at all positions and frequencies outside of the scatterers is available [4,33]. Practically speaking, we can only measure the field at a finite number of locations as well as a limited number of frequencies.

As a result, the solution is always nonunique for practical problems [4,33]. In order to overcome the nonuniqueness of the solution, a fast, accurate, and inexpensive apparatus for the generation of the interrogating field and the measurement of a large number of samples of the scattered field is necessary.

**Fig. 2.1** Multiple scattering

*III. Stable:* The inverse scattering problem may be unstable because a small arbitrary change in the incident field may result in an arbitrarily large change in the material parameters.

From a practical perspective, the measured scattered field is always corrupted by noise, and therefore, the solution might become unstable. Besides noise, the solution is very dependent on the observation point locations and the measurement accuracy.

After all, because of the nonuniqueness and instability of the inverse scattering problem, it is considered an ill-posed problem.

### 2.1.2 Nonlinearity of the Inverse Scattering Problem

In an inverse scattering problem, the aim is to determine the dielectric properties in the imaging domain from the knowledge of the scattered field.

In Eq. (2.2), the second term represents the multiplication of the field and material properties which means there is a nonlinear relation between field and material properties. When the scattered fields are only available at discrete points, this problem becomes more severe. Another reason for nonlinearity is the multiple reflections from different boundaries (Fig. 2.1).

Significant absorption of the incident field may occur in heterogeneous object with high conductivity. For dispersive objects, different components of the signal travel at different speeds; thus the shape of the original waveform is altered. The abovementioned characteristics make the inverse problem nonlinear and complicated to solve.

In summary, any algorithm used in order to solve the inverse scattering problems needs to consider three fundamental factors:

1. How to deal with the ill-posed and the ill-conditioned inverse scattering problems which is possible by using an iterative algorithm.
2. Developing an efficient accurate numerical method as forward solver can be computationally intensive.

3. Overcoming the drawbacks of two previous factors can be done using parallel computing power.

In this chapter we will address the first and second factors. We will discuss the third factor in Chap. 4.

### 2.1.3 Inverse Scattering Problem from Theoretical Point of View

Consider an OI inside the imaging chamber. The cross section of the OI successively is irradiated by a number of  $E_{\text{inc}}(\mathbf{r}, \omega, \Phi)$ . The electric field is calculated at the receivers and can be expressed in functional form as  $E_{\text{total}}(\mathbf{r}, \omega, \epsilon(\mathbf{r}, \omega), \sigma(\mathbf{r}, \omega))$  where functions  $\epsilon(\mathbf{r}, \omega)$  and  $\sigma(\mathbf{r}, \omega)$  are the unknown distributions of permittivity and conductivity, respectively.  $\mathbf{r}$  is the spatial coordinate.

The goal is to find a set of dielectric properties of the material that can generate the same scattered fields as the measured ones. The following condition needs to be satisfied:

$$\sum_{i=1}^M |E_{\text{total}}^{\text{estimated}}(\mathbf{r}_i, \omega, \epsilon(\mathbf{r}, \omega), \sigma(\mathbf{r}, \omega)) - E_{\text{total}}^{\text{measured}}(\mathbf{r}_i, \omega)| = 0, \quad (2.8)$$

where  $E_{\text{total}}^{\text{measured}}(\mathbf{r}_i, \omega)$  is the measured total field at the  $M$  number of receiver points and the  $E_{\text{total}}^{\text{estimated}}(\mathbf{r}_i, \omega, \epsilon(\mathbf{r}, \omega), \sigma(\mathbf{r}, \omega))$  is the total field computed by the forward solver. It is worth noting that inverse scattering is an overdetermined problem. There might be several arrangements of scatterers that will have very similar field values at the sampling points. There is always need for additional methods to examine if the solution physically feasible. The next section is devoted to introducing an iterative technique in order to find the permittivity and conductivity profiles that satisfies Eq. (2.8).

## 2.2 Iterative Technique

Iterative techniques are currently one of the best options for solving the nonlinear inverse scattering problem. These techniques have a greater probability of converging to the right solution. In this approach the scattered field outside the object is measured and the differences between this field and the scattered field of a possible solution calculated by a forward solver is minimized. Therefore, this approach needs an iterative minimization process. Figure 2.2 shows the flowchart of the iterative technique for the image reconstruction method. This method is based on optimizing a fitness function (or cost function) (2.8):

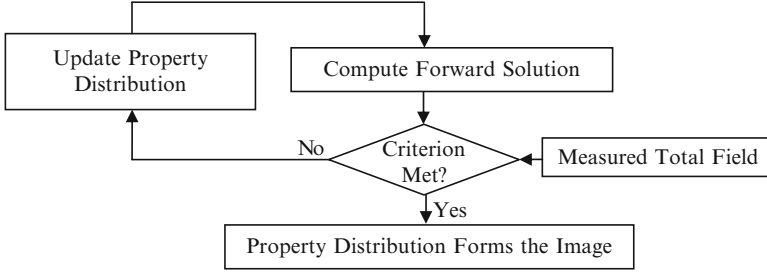


**Fig. 2.2** Flowchart of the iterative technique

$$\min_{\mathbf{r}, \omega, \epsilon(\mathbf{r}, \omega), \sigma(\mathbf{r}, \omega)} \alpha \left\| E_{\text{total}}^{\text{estimated}}(\mathbf{r}_i|_{i=1}^M, \omega, \epsilon(\mathbf{r}, \omega), \sigma(\mathbf{r}, \omega)) \right\| - \beta \left\| E_{\text{total}}^{\text{measured}}(\mathbf{r}_i|_{i=1}^M, \omega) \right\| + R(\omega, \epsilon(\mathbf{r}, \omega), \sigma(\mathbf{r}, \omega)). \quad (2.9)$$

The constants  $\alpha$  and  $\beta$  can be heuristically determined for a certain class of scatterers. This kind of calibration is based on the assumption that a certain class of scatterers can be inspected and the optimal values found for  $\alpha$  and  $\beta$  can be used for a class of similar scatterers. In the third term of Eq. (2.9), the function  $R(\omega, \epsilon(\mathbf{r}, \omega), \sigma(\mathbf{r}, \omega))$  is a term that can include *a priori* information (constraints of dielectric properties) or their gradient configuration to be inspected and can play the role of regularization. The general approach for regularizing an ill-posed problem is to set “appropriate” constraints on the solution, e.g., limiting the norm of the solution or enforcing the solution to lie in an appropriate subspace [5]. This term is needed because of the ill-posedness of the inverse problem, and in this book, *a priori* information is used as regularization term.

## 2.3 Time Domain Algorithm

The majority of the proposed inverse scattering algorithms have used monochromatic (single-frequency) excitation [6–16]. Although using monochromatic incidences has been applied successfully to different applications of MWI, it has a significant shortcoming. It has been proven that due to the ill-posedness and non-linearity of the problem the inverse algorithms fail if they only use monochromatic incidences [17]. The frequency-hopping algorithm has been proposed to overcome this problem [18–23]. In this method, for the data acquisition, a continuous incident wave spectrum is necessary to illuminate the object at different frequencies and also UWB probe is required to collect the electric field. Consequently, for analyzing such a measurement setup with multiple frequencies, it is better to use a time domain solver. This is the reason that we select the time domain numerical method as the forward solver.

### 2.3.1 Time Domain Forward Scattering Problem

The goal is to calculate the scattered fields when the object, background medium, and source are completely known. This is called the forward scattering problem. In order to solve this problem, the same as the inverse problem, Maxwell's equations need to be used. For calculating the scattered field in some problems the analytical solutions, in the form of eigenfunction expansions, are available. However, when the geometry of the scatterer is complex, these analytical methods are not applicable. In such cases, we have to use approximations and/or numerical methods. Throughout this book, the FDTD numerical method has been proposed as a forward solver.

FDTD is a numerical method used to solve Maxwell's equations in the time domain by applying central difference to time and space derivation in a wide range of applications [24].

One benefit of the time domain approach is that it yields a broadband output from a single execution of the program. However, the main reason for using the FDTD approach is its effectiveness as a technique for calculating electromagnetic fields in multilayer inhomogeneous objects. With a large number of unknown parameters related to the object under the test, the FDTD approach outpaces other methods in efficiency and provides accurate results of the field penetration into objects. In FDTD methods, Maxwell's equations are solved in a closed area. This means that the solution area for scattering problems in an infinite space, such as the one that we are dealing with, needs to be truncated by an absorbing boundary condition (ABC) [24]. We chose to use the uniaxial perfectly match layer (UPML) which is a very efficient ABC [25]. The UPML ABC is based on an artificial absorbing layer surrounding the simulation region (see [24] for more details).

## 2.4 Debye Model

The frequency dependence of materials can be efficiently described in the time domain using Debye or Lorentz models [24]. These models can be expressed in different orders. The higher-order models can accurately represent arbitrary dispersive medium at the expense of computational cost and complexity [26]. The Debye equation is given by

$$\epsilon_r(\omega) = \epsilon_\infty + \sum_{p=0}^{p_{\max}} \frac{(\epsilon_s - \epsilon_\infty)}{1 + (j\omega\tau_p)^{1-\alpha_p}} - j \frac{\sigma_s}{\omega\epsilon_0}, \quad (2.10)$$

where  $\alpha_p$  is a dimensionless weight,  $\tau_p$  is the relaxation time of the  $p$ th Debye function,  $\epsilon_0$  is the permittivity of the free space,  $\epsilon_s$  and  $\epsilon_\infty$  are the dielectric constants at zero (static) and infinite frequencies, respectively.  $\sigma_s$  is the conductivity

at low frequency, and  $\omega$  is the angular frequency. In order to maintain the simplicity of the method and to reduce computational cost, the first-order Debye model is employed [27, 28]. If  $p = 0$  and  $\alpha_0 = 0$ , therefore,

$$\epsilon_r - j \frac{\sigma}{\omega \epsilon_0} = \epsilon_\infty + \frac{\epsilon_s - \epsilon_\infty}{1 + j\omega\tau_0} - j \frac{\sigma_s}{\omega \epsilon_0}, \quad (2.11)$$

$$\epsilon = \epsilon_0(\epsilon' - j\epsilon'') = \epsilon_0 \left( \epsilon' - \frac{j\sigma}{\omega \epsilon_0} \right) = \epsilon_0 \epsilon' (1 - \tan \delta), \quad (2.12)$$

$$\epsilon = \epsilon_0 \left( \epsilon_\infty + \frac{\epsilon_s - \epsilon_\infty}{1 + j\omega\tau_0} - j \frac{\sigma_s}{\omega \epsilon_0} \right). \quad (2.13)$$

From Eq. (2.13), it is evident that the permittivity is a function of frequency as well as conductivity.

## 2.5 Fundamentals of FDTD Method (Yee Algorithm)

In this book the interactions between the pulse and the multilayer dispersive objects have been modeled by FDTD method in a manner described in [24]. Being compared with the IE formulation or other numerical methods used as forward solver, the FDTD approach is very efficient for modeling inhomogeneous objects and complex geometries. The Yee-cell (Fig. 2.3) technique is implemented in the FDTD code for modeling the shape of the cylindrical object more closely. This method uses a staggered grid approximation for solving the Maxwell's equations [29]. The Yee-cell allows the properties of the medium including the permittivity, permeability, and conductance to be presented as a discrete grid. In this way the domain can be

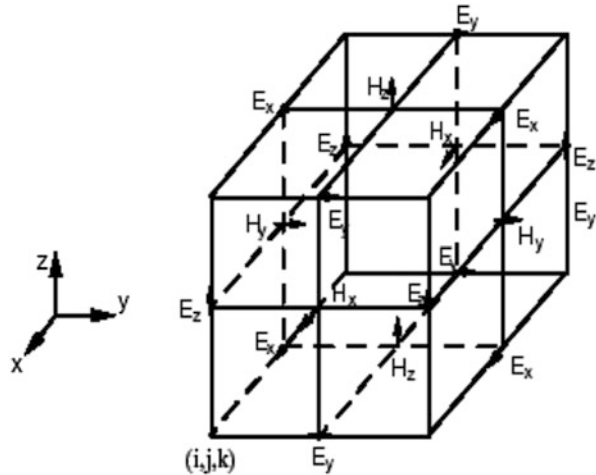


Fig. 2.3 Yee-cell schematic

divided into areas with different properties by defining the cell parameters in each area. This allows the FDTD solver to incorporate the heterogeneity by defining the dielectric properties cell by cell. The differential operators required for calculating the explicit update equations have their simplest form in rectangular coordinates and when working with plane waves this coordinate system is the obvious choice for expressing such waves. Therefore, rectangular coordinates as well as plane waves as the incident field have been chosen. In order to model the complex shape composed of varying curve surfaces, the staircasing method has been used [24]. In this method the curved surface is represented by approximating its trajectory with a series of steps in the grid. This approximation does not work very well for a small radius of curvature. One way to make it better is to introduce a smaller cell size which leads to high computational requirements. The following cell size was used for all simulations:  $\Delta x = \Delta y = \lambda_{\min}/20$ .

$$\lambda_{\min} = \frac{C_{\text{background}}}{f_{\max}}, \quad (2.14)$$

where  $C_{\text{background}}$  is the velocity of propagation,  $f_{\max}$  is the maximum value of the frequency components of the excitation signal (e.g., a modulated or differentiated Gaussian pulse), and  $\Delta x$  and  $\Delta y$  are the cell size in  $x$  and  $y$  direction [24]. In fact, for designing the mesh size, we must take into account the required bandwidth and the available computational power. In addition, the cell size also relates to runtime.

The time step is calculated given the cell sizes and the speed of the propagation of the wave in the free space. The time increment  $\Delta t$  is equal to 0.98 of the Courant stability limit. The Courant stability limit is given by

$$\Delta t \leq \frac{1}{C_{\text{background}} \sqrt{\left(\frac{1}{\Delta x}\right)^2 + \left(\frac{1}{\Delta y}\right)^2}}. \quad (2.15)$$

Thus, the smaller the cell sizes, the smaller the associated time steps leading to the longer runtime. The proposed MWT technique requires wideband pulse for high-resolution imaging. The incident wave used in this book is a Gaussian pulse given by

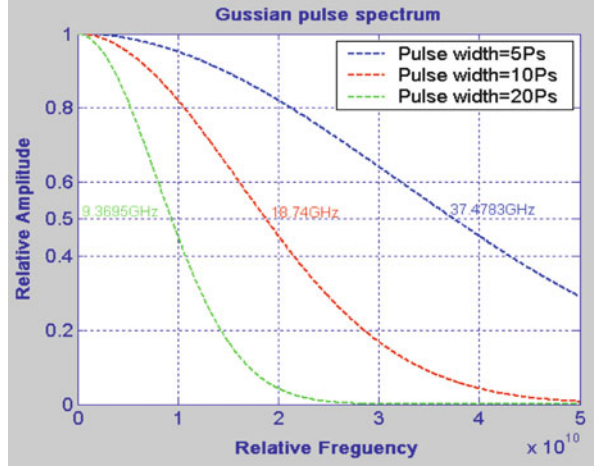
$$G(t) = \exp\left[-(t - t_0)^2/2\tau_p^2\right], \quad (2.16)$$

where  $\tau_p$  is the pulse width. The frequency spectrum of Gaussian pulse is given by

$$G(\omega) = \sqrt{2\pi\tau_p} \exp\left[-(\omega\tau_p)^2/2\right]. \quad (2.17)$$

Figure 2.4 shows the Gaussian pulse spectrum for three different pulse widths and Table 2.1 indicates the pulse duration for different bandwidth. Depending on the bandwidth that we are interested in, the corresponding pulse duration needs to be used.

Different parts of the 2D model are shown in Fig. 2.5. In the central region, both incident and scattered fields exist ( $E_{\text{total}} = E_{\text{scat}} + E_{\text{inc}}$ ) and this is called the total

**Fig. 2.4** Gaussian pulse spectrum**Table 2.1** Pulse duration versus bandwidth frequency

Pulse duration (ps)	Gaussian bandwidth (GHz)
1	186.8
2	93.42
5	37.37
10	18.68
20	9.34

field (TF) region. Any structure under the test should be in this region. The next region contains only the scattered field which is called scattered field (SF) region. The TF and SF regions are separated by a nonphysical virtual surface that serves to connect the fields in each region and thereby generates the incident wave. The transmitting antennas are posed at the boundary separating TF region and SF region. We used the TF/SF formulation, which makes the values of scattered field directly obtainable from the FDTD code [24]. Typically, the scattered field is calculated by subtracting the total field from incident field ( $E_{\text{scat}} = E_{\text{total}} - E_{\text{inc}}$ ). However, by using the TF/SF formulation, the scattered field can be calculated directly without extra processing [24]. The magnitude of the fields at the TF region, when the background is free space ( $\sigma = 0.0 \text{ S/m}$ ,  $\epsilon_r = 1.0$ ), is

$$E_{zx,\text{total}}|_{i,j}^{n+1} = E_{zx,\text{total}}|_{i,j}^n + \frac{\Delta t}{\epsilon_0 \Delta x} [H_{y,\text{total}}|_{i,j}^{n+\frac{1}{2}} - H_{y,\text{total}}|_{i-1,j}^{n+\frac{1}{2}}], \quad (2.18)$$

$$E_{zy,\text{total}}|_{i,j}^{n+1} = E_{zy,\text{total}}|_{i,j}^n - \frac{\Delta t}{\epsilon_0 \Delta y} [H_{x,\text{total}}|_{i,j}^{n+\frac{1}{2}} - H_{x,\text{total}}|_{i,j-1}^{n+\frac{1}{2}}], \quad (2.19)$$

$$H_{x,\text{total}}|_{i,j}^{n+\frac{1}{2}} = H_{x,\text{total}}|_{i,j}^{n-\frac{1}{2}} - \frac{\Delta t}{\mu_0 \Delta y} [E_{zx,\text{total}}|_{i,j+1}^n + E_{zy,\text{total}}|_{i,j+1}^n - E_{zx,\text{total}}|_{i,j}^n - E_{zy,\text{total}}|_{i,j}^n], \quad (2.20)$$

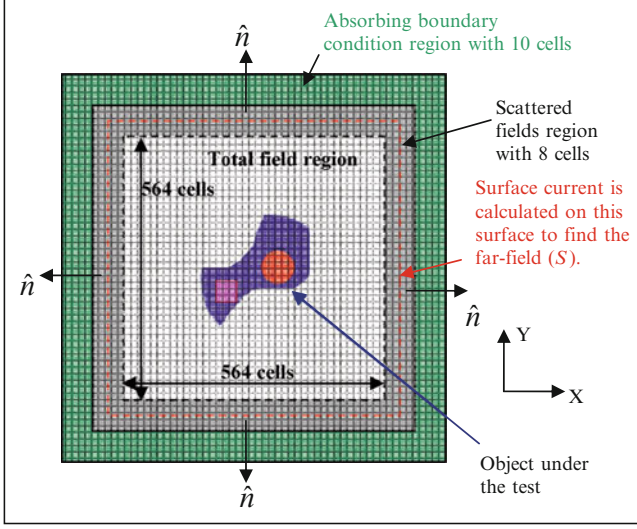


**Fig. 2.5** Different regions of solution space

$$H_{y,\text{total}}|_{i,j}^{n+\frac{1}{2}} = H_{y,\text{total}}|_{i,j}^{n-\frac{1}{2}} + \frac{\Delta t}{\mu_0 \Delta x} [E_{zx,\text{total}}|_{i+1,j}^n + E_{zy,\text{total}}|_{i+1,j}^n - E_{zx,\text{total}}|_{i,j}^n - E_{zy,\text{total}}|_{i,j}^n]. \quad (2.21)$$

The magnitude of the field at the SF region with free space background ( $\sigma = 0.0 \text{ S/m}$ ,  $\epsilon_r = 1.0$ ) is

$$E_{zx,\text{scat}}|_{i,j}^{n+1} = E_{zx,\text{scat}}|_{i,j}^n + \frac{\Delta t}{\epsilon_0 \Delta x} [H_{y,\text{scat}}|_{i,j}^{n+\frac{1}{2}} - H_{y,\text{scat}}|_{i-1,j}^{n+\frac{1}{2}}] \quad (2.22)$$

$$E_{zy,\text{scat}}|_{i,j}^{n+1} = E_{zy,\text{scat}}|_{i,j}^n - \frac{\Delta t}{\epsilon_0 \Delta y} [H_{x,\text{scat}}|_{i,j}^{n+\frac{1}{2}} - H_{x,\text{scat}}|_{i,j-1}^{n+\frac{1}{2}}] \quad (2.23)$$

$$H_{x,\text{scat}}|_{i,j}^{n+\frac{1}{2}} = H_{x,\text{scat}}|_{i,j}^{n-\frac{1}{2}} - \frac{\Delta t}{\mu_0 \Delta y} [E_{zx,\text{scat}}|_{i,j+1}^n + E_{zy,\text{scat}}|_{i,j+1}^n - E_{zx,\text{scat}}|_{i,j}^n - E_{zy,\text{scat}}|_{i,j}^n] \quad (2.24)$$

$$H_{y,\text{scat}}|_{i,j}^{n+\frac{1}{2}} = H_{y,\text{scat}}|_{i,j}^{n-\frac{1}{2}} + \frac{\Delta t}{\mu_0 \Delta x} [E_{zx,\text{scat}}|_{i+1,j}^n + E_{zy,\text{scat}}|_{i+1,j}^n - E_{zx,\text{scat}}|_{i,j}^n - E_{zy,\text{scat}}|_{i,j}^n] \quad (2.25)$$

and also at the TF region the relationship between the total field and scattered field is

$$E_{\text{total}} = E_{\text{scat}} + E_{\text{inc}}, \quad (2.26)$$

$$H_{\text{total}} = H_{\text{scat}} + H_{\text{inc}}. \quad (2.27)$$

Based on the consistency condition, the magnitude of fields at the boundary between TF region and SF region should be as follows:

*At front face of TF region ( $j = j_0; i = i_0, \dots, i_1$ )*

From the continuity of tangential magnetic field at the boundary:

$$H_{x,\text{total}}|_{i,j_0+\frac{1}{2}}^{n+\frac{1}{2}} = H_{x,\text{scat}}|_{i,j_0-\frac{1}{2}}^{n+\frac{1}{2}}, \quad (2.28)$$

$$E_{zy}|_{i,j_0}^{n+1} = \left\{ E_{zy}|_{i,j_0}^{n+1} \right\} + \frac{\Delta t}{\epsilon_0 \Delta y} [H_{x,\text{inc}}|_{i,j_0-\frac{1}{2}}^{n+\frac{1}{2}}]. \quad (2.29)$$

*At back face of TF region ( $j = j_1; i = i_0, \dots, i_1$ )*

From the continuity of tangential magnetic field at the boundary:

$$H_{x,\text{scat}}|_{i,j_1+\frac{1}{2}}^{n+\frac{1}{2}} = H_{x,\text{total}}|_{i,j_1-\frac{1}{2}}^{n+\frac{1}{2}}, \quad (2.30)$$

$$E_{zy}|_{i,j_1}^{n+1} = \left\{ E_{zy}|_{i,j_1}^{n+1} \right\} - \frac{\Delta t}{\epsilon_0 \Delta y} [H_{x,\text{inc}}|_{i,j_1+\frac{1}{2}}^{n+\frac{1}{2}}]. \quad (2.31)$$

*At left face of TF region ( $i = i_0; j = j_0, \dots, j_1$ )*

From the continuity of tangential magnetic field at the boundary:

$$H_{y,\text{total}}|_{i_0+\frac{1}{2},j}^{n+\frac{1}{2}} = H_{y,\text{scat}}|_{i_0-\frac{1}{2},j}^{n+\frac{1}{2}}, \quad (2.32)$$

$$E_{zx}|_{i_0,j}^{n+1} = \left\{ E_{zx}|_{i_0,j}^{n+1} \right\} - \frac{\Delta t}{\epsilon_0 \Delta x} [H_{y,\text{inc}}|_{i_0-\frac{1}{2},j}^{n+\frac{1}{2}}]. \quad (2.33)$$

*At right face of TF region ( $i = i_1; j = j_0, \dots, j_1$ )*

From the continuity of tangential magnetic field at the boundary:

$$H_{y,\text{scat}}|_{i_1+\frac{1}{2},j}^{n+\frac{1}{2}} = H_{y,\text{total}}|_{i_1-\frac{1}{2},j}^{n+\frac{1}{2}}, \quad (2.34)$$

$$E_{zx}|_{i_1,j}^{n+1} = \left\{ E_{zx}|_{i_1,j}^{n+1} \right\} + \frac{\Delta t}{\epsilon_0 \Delta x} [H_{y,\text{inc}}|_{i_1+\frac{1}{2},j}^{n+\frac{1}{2}}]. \quad (2.35)$$

*At outside front face of TF region ( $j = j_0 - 1/2; i = i_0, \dots, i_1$ )*

From the continuity of tangential electric field at the boundary:

$$E_{z,\text{total}}|_{i,j_0+1}^n = E_{z,\text{scat}}|_{i,j_0}^n, \quad (2.36)$$

$$H_x|_{i,j_0-\frac{1}{2}}^{n+\frac{1}{2}} = \left\{ H_x|_{i,j_0-\frac{1}{2}}^{n+\frac{1}{2}} \right\} + \frac{\Delta t}{\mu_0 \Delta y} [E_{z,\text{inc}}|_{i,j_0}^n]. \quad (2.37)$$

*At outside back face of TF region ( $j = j_0 + 1/2; i = i_0, \dots, i_1$ )*

From the continuity of tangential electric field at the boundary:

$$E_{z,\text{scat}}|_{i,j_1}^n = E_{z,\text{total}}|_{i,j_1-1}^n, \quad (2.38)$$

$$H_x|_{i,j_1+\frac{1}{2}}^{n+\frac{1}{2}} = \left\{ H_x|_{i,j_1+\frac{1}{2}}^{n+\frac{1}{2}} \right\} - \frac{\Delta t}{\mu_0 \Delta y} [E_{z,\text{inc}}|_{i,j_1}^n]. \quad (2.39)$$

*At outside left face of TF region ( $i = i_0 - 1/2; j = j_0, \dots, j_1$ )*

From the continuity of tangential electric field at the boundary:

$$E_{z,\text{total}}|_{i_0+1,j}^n = E_{z,\text{scat}}|_{i_0,j}^n, \quad (2.40)$$

$$H_x|_{i_0-\frac{1}{2},j}^{n+\frac{1}{2}} = \left\{ H_x|_{i_0-\frac{1}{2},j}^{n+\frac{1}{2}} \right\} - \frac{\Delta t}{\mu_0 \Delta x} [E_{z,\text{inc}}|_{i_0,j}^n]. \quad (2.41)$$

*At outside right face of total field region ( $i = i_1 + 1/2; j = j_0, \dots, j_1$ )*

From the continuity of tangential electric field at the boundary:

$$E_{z,\text{scat}}|_{i_1,j}^n = E_{z,\text{total}}|_{i_1,j}^n, \quad (2.42)$$

$$H_y|_{i,j_1+\frac{1}{2}}^{n+\frac{1}{2}} = \left\{ H_y|_{i,j_1+\frac{1}{2}}^{n+\frac{1}{2}} \right\} + \frac{\Delta t}{\mu_0 \Delta x} [E_{z,\text{inc}}|_{i_1,j}^n]. \quad (2.43)$$

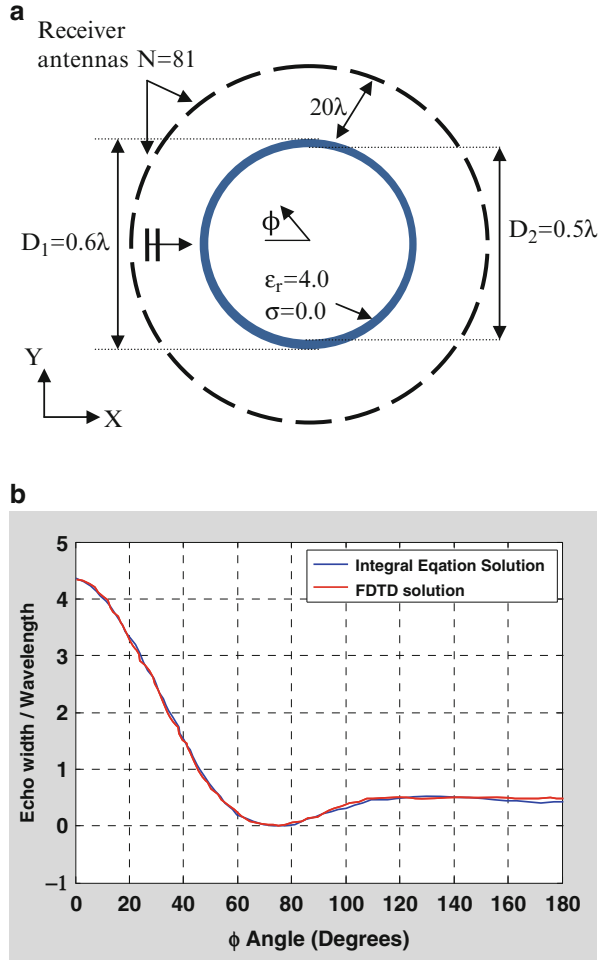
In order to show the accuracy of the FDTD method used to determine the scattered field, two examples with two different methods are provided. In the first example we compare the scattered field calculated with FDTD and the scattered field computed with the Richmond procedure [30]. In this example the dielectric shell cylinder has a permittivity of 4 and no conductivity with inner diameter equal to  $0.5\lambda$  and  $0.6\lambda$  outer diameter (Fig. 2.6a). Eighty-one observation points are assigned around the shell cylinder to calculate the scattered field in the far-field zone. The 2D near-field to far-field transformation is developed based on [24]. The same as other examples in this book, ten layers UPML ABC are used for these two simulations. Figure 2.6b shows the scattered field at 2.5 GHz using the FDTD compared with IE solution.

Figure 2.7a shows another example for a lossy dielectric cylinder with permittivity (1) and conductivity ( $1.57 \text{ S/m}$ ) with radius  $0.53\lambda$  and 100 receiver probes in the far-field zone. Figure 2.7b shows the scattered field at 2.5 GHz using the FDTD and MoM method [31], respectively.

## 2.6 Frequency-Dependent FDTD

The conventional FDTD has been previously used for the modeling of nondispersive material using constant material parameters. Frequency-dependent finite-difference time domain ((FD)<sup>2</sup>TD) is an extended version of the conventional FDTD that incorporates the Debye model into the difference equations and can handle dispersive

**Fig. 2.6** (a) Dielectric shell cylinder with 81 observation points, (b) distant scattering pattern of circular dielectric cylinder illuminated by plane wave



materials more accurately [32]. In this section it is explained how the Debye model has been implemented into the FDTD numerical model. By taking the inverse Fourier transform of Eqs. (2.13), (2.5), and (2.6), one obtained  $\epsilon(t)$ ,  $\mathbf{B}(t)$ , and  $\mathbf{D}(t)$ :

$$\epsilon(t) = \epsilon_\infty \delta(t) + \frac{\epsilon_0 - \epsilon_\infty}{\tau_0} e^{-t/\tau_0} u(t), \quad (2.44)$$

$$\mathbf{B}(t) = \mu_0 \mathbf{H}(t), \quad (2.45)$$

$$\mathbf{D}(t) = \int_{-\infty}^{+\infty} \epsilon(t - \beta) \mathbf{E}(\beta) d\beta. \quad (2.46)$$

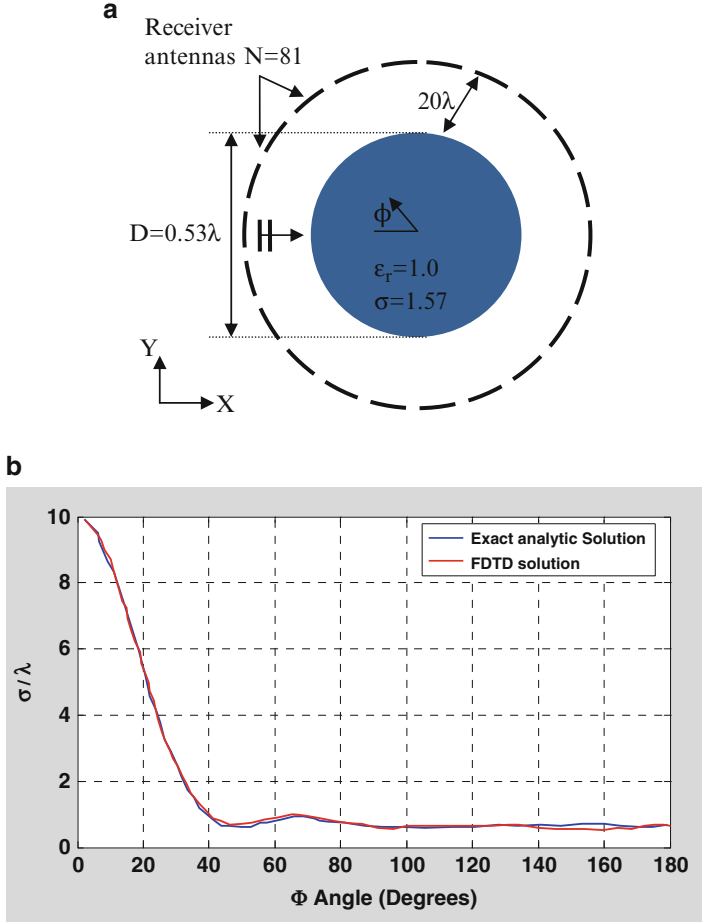


**Fig. 2.7** (a) Lossy circular cylinder, (b) TM plot of  $2\pi|E_{\text{scat}}|^2/\lambda$  against  $\Phi$  for case of lossy circular cylinder at 2.5 GHz frequency

Therefore, the electric flux density is

$$\mathbf{D}(t) = \epsilon_{\infty} \mathbf{E}(t) + \frac{\epsilon_0 - \epsilon_{\infty}}{\tau_0} \int_{-\infty}^{+\infty} e^{-(t-\beta)/\tau_0} u(t-\beta) \mathbf{E}(\beta) d\beta. \quad (2.47)$$

By differentiating the above equation twice with respect to  $t$ , we obtain the first and second derivatives of  $D(t)$

$$\frac{\partial \mathbf{D}(t)}{\partial t} = \epsilon_{\infty} \frac{\partial \mathbf{E}(t)}{\partial t} + \frac{\epsilon_0 - \epsilon_{\infty}}{\tau_0} \left[ E(t) - \frac{\Delta t}{\tau_0} \mathbf{S}(t) \right], \quad (2.48)$$

$$\frac{\partial^2 \mathbf{D}(t)}{\partial t^2} = \epsilon_{\infty} \frac{\partial^2 \mathbf{E}(t)}{\partial t^2} + \frac{\epsilon_0 - \epsilon_{\infty}}{\tau_0} \left[ \frac{\partial \mathbf{E}(t)}{\partial t} - \frac{1}{\tau_0} \mathbf{E}(t) + \frac{\Delta t}{\tau_0^2} \mathbf{S}(t) \right], \quad (2.49)$$

where

$$\mathbf{S}(t) = \frac{1}{\Delta t} \int_{-\infty}^{+\infty} e^{-(t-\beta)/\tau_0} \mathbf{u}(t-\beta) \mathbf{E}(\beta) d\beta \quad (2.50)$$

$\mathbf{S}(t)$  can be reduced to recursive form which is

$$\mathbf{S}(t) = e^{-\Delta t/\tau_0} \mathbf{S}(t - \Delta t) + \frac{1}{2} [e^{-\Delta t/\tau_0} \mathbf{E}(t - \Delta t) + \mathbf{E}(t)]. \quad (2.51)$$

Applying Eqs. (2.48) and (2.49) to the time domain form of Eqs. (2.1) and (2.2), we obtained the magnetic field,  $H$ , and electric field,  $E$ , in finite-difference form as

$$\begin{aligned} E_z^{n+1}(i, j) = & \left[ 1 - \Delta t \left( \frac{\sigma_s}{\epsilon_\infty} + \frac{\epsilon_0 - \epsilon_\infty}{\epsilon_\infty \tau_0} \right) \right] E_z^n(i, j) \\ & + \frac{\Delta t}{\epsilon_\infty \Delta x} \left[ H_y^{n+\frac{1}{2}} \left( i + \frac{1}{2}, j \right) - H_y^{n+\frac{1}{2}} \left( i - \frac{1}{2}, j \right) \right] \\ & - \frac{\Delta t}{\epsilon_\infty \Delta y} \left[ H_x^{n+\frac{1}{2}} \left( i, j + \frac{1}{2} \right) - H_x^{n+\frac{1}{2}} \left( i, j - \frac{1}{2} \right) \right] \\ & + \left( \frac{\epsilon_0 - \epsilon_\infty}{\epsilon_\infty} \right) (\omega_0 \Delta t)^2 S_z^n(i, j), \end{aligned} \quad (2.52)$$

$$S_z^{(n)}(i, j) = e^{-\Delta t/\tau_0} S_z^{(n-1)}(i, j) + \frac{1}{2} [e^{-\Delta t/\tau_0} E_z^{(n-1)}(i, j) + E_z^n(i, j)]. \quad (2.53)$$

The magnetic field equations remain unchanged as

$$\begin{aligned} H_x^{n+\frac{1}{2}} \left( i, j + \frac{1}{2} \right) = & H_x^{n-1/2} \left( i, j + \frac{1}{2} \right) \\ & - \frac{\Delta t}{\mu_0 \Delta x} [E_z^n(i, j + 1) - E_z^n(i, j)], \end{aligned} \quad (2.54)$$

$$\begin{aligned} H_y^{n+\frac{1}{2}} \left( i + \frac{1}{2}, j \right) = & H_y^{n-1/2} \left( i + \frac{1}{2}, j \right) \\ & + \frac{\Delta t}{\mu_0 \Delta y} [E_z^n(i + 1, j) - E_z^n(i, j)]. \end{aligned} \quad (2.55)$$

Since we used the first-order Debye equation to describe the dispersive material, the electric field values only at the previous time step are needed to be stored. However, using a higher-order Debye model requires storing a large number of electric field values at previous time steps which consequently increases the computational complexity.

An  $(\text{FD})^2\text{TD}$  program was developed to simulate the interaction of the plane wave with materials and evaluate the scattered field. The program is written for a 2D Cartesian coordinate system. Unless otherwise noted, all forward simulations in this book are performed by the  $(\text{FD})^2\text{TD}$  numerical method. From a computational point of view, the inverse scattering program has a long runtime because it is computationally heavy. By using a parallel computer and through message passing interface (MPI) method, the runtime can be decreased in inverse proportion to the number of parallel processors used for the  $(\text{FD})^2\text{TD}$  solver. The parallel  $(\text{FD})^2\text{TD}$  will be explained in Chap. 6.

## References

1. R. Harrington, *Time-Harmonic Electromagnetic Fields* (IEEE Press, New York 2001)
2. F. Ahmad, M. Amin, S. Kassam, Synthetic aperture beamformer for imaging through a dielectric wall. *IEEE Trans. Aero. Electron. Syst.* **41**(1), 271–283 (2005)
3. J. Hadamard, *Lectures on Cauchy's Problem in Linear Partial Differential Equations* (Yale University Press, New Haven, 1923)
4. M. Oristaglio, H. Blok, *Wavefield Imaging and Inversion in Electromagnetics and Acoustics*. Course Notes TU Delft, 1995
5. P. Mojab, J. LoVetri, Overview and classification of some regularization techniques for the gauss-newton inversion method applied to inverse scattering problems. *IEEE Trans. Antenn. Propag.* **57**(9), 2658–2665 (2009)
6. W. Chew, Y. Wang, Reconstruction of two-dimensional permittivity distribution using the distorted born iterative method. *IEEE Trans. Med. Imag.* **9**(2), 218–225 (1990)
7. S. Caorsi, G. Gragnani, M. Pastorino, Two-dimensional microwave imaging by a numerical inverse scattering solution. *IEEE Trans. Microw. Theor. Tech.* **38**(8), 981–990 (1990)
8. R.E. Kleinman, P.M. Van den Berg, A modified gradient method for two-dimensional problems in tomography. *J. Comput. Appl. Math.* **42**(1), 17–35 (1992)
9. A. Franchois, C. Pichot, Microwave imaging-complex permittivity reconstruction with a levenberg-marquardt method. *IEEE Trans. Antenn. Propag.* **45**(2), 203–215 (1997)
10. P. Meaney, K. Paulsen, T. Ryan, Two-dimensional hybrid element image reconstruction for tm illumination. *IEEE Trans. Antenn. Propag.* **43**(3), 239–247 (1995)
11. I.T. Rekanos, T.D. Tsiboukis, An iterative numerical method for inverse scattering problems. *Radio Sci.* **34**(6), 1401–1412 (1999)
12. W. Chien, C.C. Chiu, Using nu-ssga to reduce the searching time in inverse problem of a buried metallic object. *IEEE Trans. Antenn. Propag.* **53**(10), 3128–3134 (2005)
13. A. Qing, An experimental study on electromagnetic inverse scattering of a perfectly conducting cylinder by using the real-coded genetic algorithm. *Microw. Opt. Tech. Lett.* **30**, 315–320 (2001)
14. S. Caorsi, A. Massa, M. Pastorino, A computational technique based on a real-coded genetic algorithm for microwave imaging purposes. *IEEE Trans. Geosci. Rem. Sens.* **38**(4), 1697–1708 (2000)
15. T. Takenaka, Z.Q. Meng, T. Tanaka, W.C. Chew, Local shape function combined with genetic algorithm applied to inverse scattering for strips. *Microw. Opt. Tech. Lett.* **16**, 337–341 (1997)
16. V. Thomas, C. Gopakumar, J. Yohannan, A. Lonappan, G. Bindu, A.V.P. Kumar, V. Ham-sakutty, K.T. Mathew, A novel technique for localizing the scatterer in inverse profiling of two dimensional circularly symmetric dielectric scatterers using degree of symmetry and neural networks. *J. Electromagn. Waves Appl.* **19**(15), 2113–2121 (2005)

17. D. Colton, R. Kress, *Inverse Acoustic and Electromagnetic Scattering Theory* (Springer, New York, 1992)
18. I.T. Rekanos, Time-domain inverse scattering using lagrange multipliers: an iterative fdtd-based optimization technique. *J. Electromagn. Waves Appl.* **17**(2), 271–289 (2003)
19. N.W. Kang, Y.S. Chung, C. Cheon, H.K. Jung, A new 2-d image reconstruction algorithm based on fdtd and design sensitivity analysis. *IEEE Trans. Microw. Theor. Tech.* **50**(12), 2734–2740 (2002)
20. T. Takenaka, H. Jia, T. Tanaka, Microwave imaging of electrical property distributions by a forward-backward time stepping method. *J. Electromagn. Waves Appl.* **14**, 1609–1625 (2000)
21. S. He, P. Fuks, G. Larson, An optimization approach to time-domain electromagnetic inverse problem for a stratified dispersive and dissipative slab. *IEEE Trans. Antenn. Propag.* **44**(9), 1277–1282 (1996)
22. W. Chew, J. Lin, A frequency-hopping approach for microwave imaging of large inhomogeneous bodies. *IEEE Microw. Guided Wave Lett.* **5**(12), 439–441 (1995)
23. I. Rekanos, T. Tsiaboukis, A finite element-based technique for microwave imaging of two-dimensional objects. *IEEE Trans. Instrum. Meas.* **49**(2), 234–239 (2000)
24. A. Taflov, S.C. Hagness, *Computational Electrodynamics: The Finite-Difference Time-Domain Method*, 3rd edn. (Artech House, Norwood, 2005)
25. J. Berenger, A perfectly matched layer for the absorption of electromagnetic waves. *J. Comput. Phys.* **114**(2), 185–200 (1994)
26. P. Kosmas, C. Rappaport, E. Bishop, Modeling with the fdtd method for microwave breast cancer detection. *IEEE Trans. Microw. Theor. Tech.* **52**(8), 1890–1897 (2004)
27. M. Converse, E. Bond, B. Veen, C. Hagness, A computational study of ultra-wideband versus narrowband microwave hyperthermia for breast cancer treatment. *IEEE Trans. Microw. Theor. Tech.* **54**(5), 2169–2180 (2006)
28. X. Li, S. Hagness, A confocal microwave imaging algorithm for breast cancer detection. *IEEE Microw. Wireless Compon. Lett.* **11**(3), 130–132 (2001)
29. K. Yee, Numerical solution of initial boundary value problems involving maxwell's equations in isotropic media. *IEEE Trans. Antenn. Propag.* **14**(3), 302–307 (1966)
30. J. Richmond, Scattering by a dielectric cylinder of arbitrary cross section shape. *IEEE Trans. Antenn. Propag.* **13**(3), 334–341 (1965)
31. M. Ouda, A. Sebak, Scattering from lossy dielectric cylinders using a multifilament current model with impedance boundary conditions. *IEE Proc. Microw. Antenn. Propag. H* **139**(5), 429–434 (1992)
32. M. Bui, S. Stuchly, G. Costache, Propagation of transients in dispersive dielectric media. *IEEE Trans. Microw. Theor. Tech.* **39**(7), 1165–1172 (1991)
33. C. Gilmore, Towards and improved microwave tomography system. Ph.D. Dissertation, Dept. Elect. Comput. Eng., Univ. of Manitoba, 2009

Microwave Tomography

Global Optimization, Parallelization and Performance  
Evaluation

Noghanian, S.; Sabouni, A.; Desell, T.; Ashtari, A.

2014, XVII, 198 p. 117 illus., 112 illus. in color.,

Hardcover

ISBN: 978-1-4939-0751-9